Low-Noise Current Sensing System for Nanopore

Sung-Jae Lee, Sang-Hyun Lee, Han-Min Song, Sung-June Byun, and Kang-Yoon Lee[a]
Department of Electrical and Computer Engineering, Sungkyunkwan University
E-mail : sungjae701@g.skku.edu, dalkuk2@g.skku.edu, gksalsgks2@g.skku.edu, steven7264@skku.edu, klee@skku.edu

***Abstract* - In this paper, a high-gain low-noise current signal detection system ASIC for biosensors is proposed. A resistive feedback transimpedance amplifier (TIA) was used for the biosensor that required a bias voltage, and the structure was designed to stably display the current flowing through the biosensor on the self-made graphical user interface (GUI) even when the bias voltage was changed. This paper introduces a proposed technique for the automatic calibration of current between sensors in an integrated biosensor featuring an array structure. The method involves controlling the gate bias voltage of the sensor to achieve the desired calibration. To optimize the circuit design, pseudo-resistors are employed, allowing for the implementation of a high-gain MOSFET resistor while minimizing the required area. Additionally, noise reduction is achieved through the utilization of a chopper technique. By using pseudo-resistors, a large resistor for high gain can be implemented as a MOSFET to reduce area, and noise is reduced using a chopper technique. The sensing circuit, specifically designed for biosensors, demonstrates exceptional performance with a gain of 160 dBΩ and input-referred noise of 4 pArms. The circuit is realized using 130 nm CMOS process technology, showcasing its feasibility in practical biosensing applications. The chip area is 17mm^2 and the power consumption is 10mW.**

***Keywords*—Biosensors, Nanopore, Gate Bias Circuit, Transimpedance Amplifier, Programmable Gain Amplifier**

I. INTRODUCTION

Application specific integrated circuit (ASIC)s for sensor applications are often used when you want to sense a current or voltage signal from a sensor. Biomedical applications demand the utilization of sensors capable of sub-nanoampere current sensing. These sensors encompass a wide range of technologies, including microneedle-based [1], film-based [2], and nanopore-based DNA analysis [3,4]. Nanopores have been used in diverse applications, including DNA analysis, amino acid analysis [5,6], ion analysis [7], protein and peptide analysis [8-11], as well as the detection of specific viruses through antibody-virus interactions [12]. Nanopores are widely employed in the detection of various biomolecules, enabling the identification of specific viruses or diseases such as cancer [13,14]. By utilizing this biomolecule detection method, nanopores can effectively modulate the current by adjusting the gate voltage or completely blocking the current flow [15-16]. Moreover, the fabrication of nanopore arrays allows for individual nanopores to interact with different viruses. By controlling each nanopore with a gate voltage, a single sensor can detect multiple viruses by analyzing the corresponding currents generated in each nanopore.

In applications involving sensors with extremely low output currents, a high-gain Transimpedance Amplifier (TIA) is commonly employed at the front end of the Application-Specific Integrated Circuit (ASIC). The TIA can utilize either resistive or capacitive feedback structures. In the case of a resistive feedback configuration, achieving low input-referred current noise and high gain necessitates the use of a large resistor. However, to avoid increasing circuit area, a widely adopted solution is the implementation of a pseudo-resistive structure, where an active element serves as the feedback network to achieve the desired resistance effect. However, this methodology may not be appropriate for scenarios in which substantial fluctuations in the input voltage or current of the TIA could arise due to alterations in the resistance value caused by either the DC voltage across the pseudo-resistor or the DC current flowing into the input. On the other hand, the capacitive feedback architecture can offer high gain while occupying a relatively smaller area. However, it is not suitable for sensors that produce DC input currents, as it is designed to process only AC input currents. Furthermore, due to the output current's dependence on the DC voltage bias, this architecture is not suitable for sensors that require precise DC voltage biasing.

In the context of a nanopore-based virus detection application, illustrated in Fig. 1., an ionic solution is employed, and a direct current (DC) voltage is applied to the nanopore array. Upon the entry of the target virus into the nanopore, it engages in an interaction with the antibody that is affixed to the nanopore. This interaction subsequently leads to a noticeable alteration in the current flow. Conversely, the non-target virus fails to bind with the antibody and passes through the nanopore without causing any current alteration. The magnitude of current change in this scenario ranges from nanoamperes to microamperes, depending on the bias voltage. Therefore, precise gain control of the Transimpedance Amplifier (TIA) is essential, necessitating a TIA with low noise and high gain to accurately differentiate the signal at the nanoampere level.
The central objective of this research paper is centered on the advancement of a current sensing and display system characterized by high gain and low noise. The input current is accurately converted into a corresponding current value by

a. Corresponding author; klee@skku.edu

Manuscript Received Nov. 6, 2023, Revised Dec. 9, 2023, Accepted Dec. 11, 2023

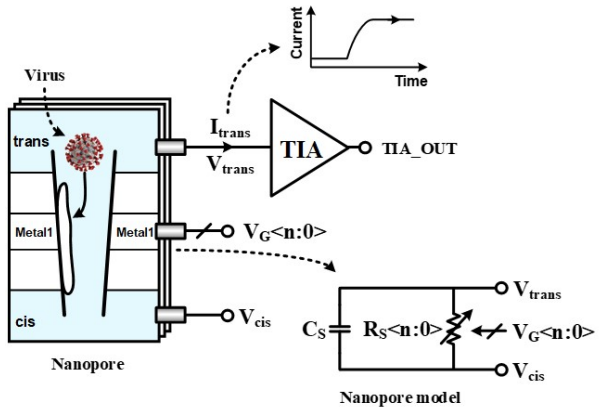

Fig. 1. Image of an nanopore array and nanopore model.

characterized by high gain and low noise. The input current is accurately converted into a corresponding current value by applying suitable range, offset, and gain values to the analog-to-digital converter (ADC) output code. This digitized output code is then utilized to plot the input current as a visual display on a portable device or laptop. To supply the sensor with a DC voltage, a resistive feedback configuration is employed, wherein a passive resistor is utilized instead of an active resistor that may exhibit varying gain characteristics with voltage. Moreover, to ensure a stable current plot even when the Transimpedance Amplifier (TIA) input voltage fluctuates, a structure is implemented, ensuring that the output voltage of the Analog Front End (AFE) remains constant. Furthermore, to minimize noise interference, a chopper technique is employed in the system design.

II. DESIGN METHODOLOGY

A. Top block diagram

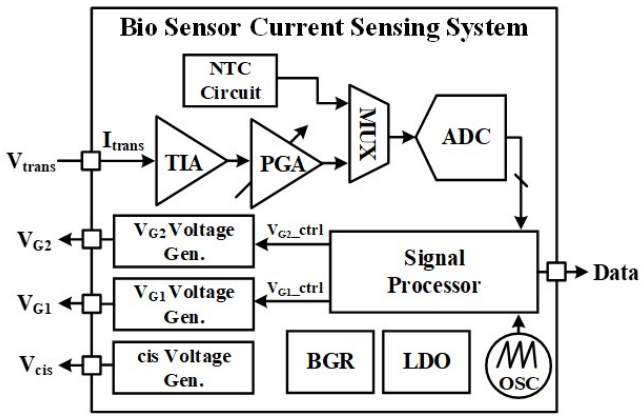

Fig. 2. Block diagram of the current sensing system for biosensor.

The current sensing system integrated circuit (IC) for the biosensor operates by capturing and processing the current flowing through the sensor. This system incorporates gain and offset compensation to accurately convert the current into identifiable digital data. When the target biomaterial attaches to the biosensor, the current passing between the drain and source undergoes modification as a result of the negative charge carried by the biomaterial.

This change in current enables the detection of the target biomaterial. The biosensor can regulate the fundamental current flowing between the drain and source by manipulating the drain voltage and gate voltage. The key components of the biosensor current sensing system IC, as illustrated in Fig. 2., include the Transimpedance Amplifier (TIA), programmable gain amplifier (PGA), analog-to-digital converter (ADC), voltage generator, negative temperature coefficient (NTC) sensor, and signal processor. The TIA is responsible for converting the current passing through the sensor into a corresponding voltage. As the current flows within the voltage supplied to the biosensor's drain, the TIA is specifically designed to provide the voltage supply while simultaneously sensing the current flowing within the supplied voltage. The PGA ensures that the voltage-converted signal matches the input range requirements of the ADC through the implementation of gain and offset compensation techniques. The ADC consists of a sigma delta modulator (SDM) architecture and a cascaded integrator comb (CIC) filter, providing 16 bits of resolution. The voltage signal from the PGA output is converted into 16-bit digital data. Temperature can be measured using an NTC sensor, as its voltage decreases when the temperature increases. The MUX(Multi-plexer) is used to reduce the area by enabling temperature sensing with one ADC. The signal processor sends the data of the bio-sensor and temperature sensor to the external environment through controlling the building blocks and serial peripheral interface (SPI) communication. The flow of current is regulated by adjusting the gate bias and the source voltage of the biosensor with a voltage generator. In particular, by adjusting the gate bias, the basic current that is different for each sensor is initially calibrated so that the same current flows.

B. Analog front end schematic

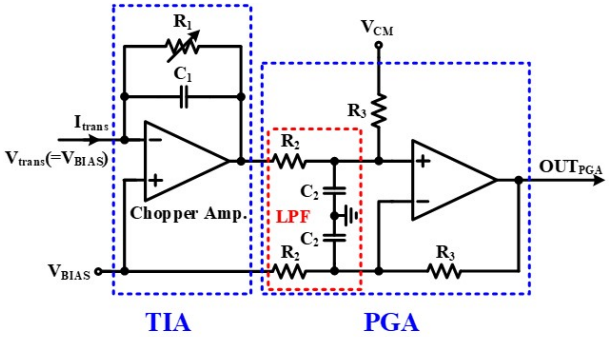

Fig. 3. Schematic of TIA and PGA.

Fig. 3. shows the proposed high-gain low-noise AFE. AFE consists of TIA and PGA. TIA converts current into voltage and achieves high gain, while PGA controls the gain and output voltage level. For high gain, TIA necessitates a very large resistor. To reduce the area, a pseudo resistor was used instead of a poly resistor to reduce the area. If the resistance for the gain is very large, a voltage offset is generated on the output due to the current flowing into the gate. This was overcome by using a chopper amplifier. To reduce noise, a

capacitor was added in parallel with the pseudo resistor so that high frequency components were not amplified. PGA uses TIA output and V_{BIAS} voltage as input. The gain can be adjusted with the R_2 resistor, and the output offset can be adjusted with the VCM voltage. The chopper circuit always needs a low pass filter to remove the chopper frequency component, so the C_2 capacitor and R_1 resistor are used as a low pass filter (LPF). With this structure of the circuit, we were able to achieve the desired gain.

C. TIA amplifier schematic

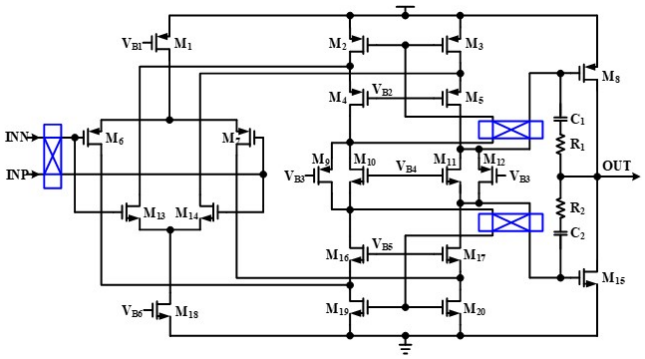

Fig. 4. Schematic of chopper amplifier used in TIA.

Fig. 4. shows the chopper amplifier circuit used in TIA. TIA has a wide input range and high gain by using a rail-to-rail folded cascode structure. There are three switching circuits that can change the phase, at the first stage input and the second stage input. If all switching circuits operate at the same frequency, even if the phase changes by 180 degrees in a single switching circuit, the original phase will be the output through two switching circuits to the output of the amplifier. If an input offset exists in the amplifier, the phase changes by 180 degrees every time it switches through a single switching circuit to the output of the amplifier, which appears as a pulse waveform. The input offset of the amplifier can be modulated by the switching frequency, and this modulation can be eliminated by utilizing a LPF at the output of the amplifier. Since LPF is used, the switching frequency must be higher than the signal frequency to maintain the sensor signal as it is.

D. Gate bias schematic

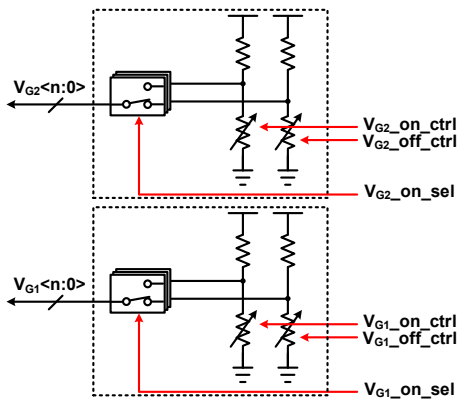

Fig. 5. Schematic of gate bias circuit.

Fig. 5 shows a block diagram of gate bias circuit that provides a gate voltage. Since the current flows only to holes in which the voltage of both rows and columns is high among the various holes of the sensor, only the current of the selected hole can be checked by adjusting the voltage of both rows and columns. Only one of the N SPDTs is connected to a high voltage corresponding to "ON", and the others are connected to a low voltage corresponding to "OFF". The ON voltage and OFF voltage nodes are connected to the SPDT respectively, and the ON voltage or OFF voltage can be finely adjusted by adjusting the resistance.

E. Current calibration flow chart

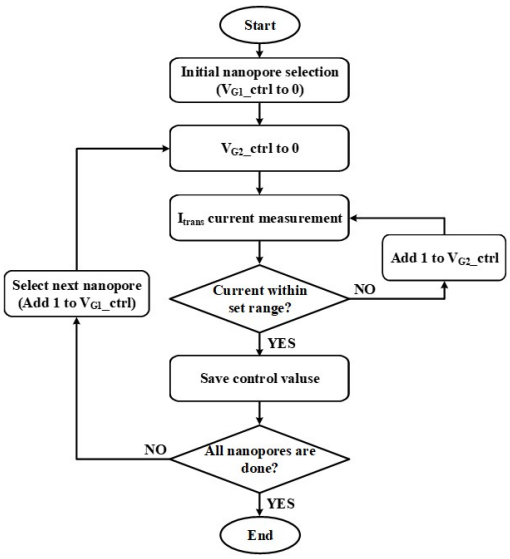

Fig. 6. Flowchart of current mismatch calibration.

Biosensor is composed of several nanopores, and the gate bias voltage applied to each nanopore can block the current flowing through the nanopore like a switch, and the current flowing through it can be controlled by adjusting the size of the voltage. To ensure that the initial current flowing through all nanopores is the same, the gate bias voltage is adjusted to calibrate each nanopore's individual initial current. Fig. 6 shows the flowchart of current mismatch calibration. After one nanopore is selected as the gate bias voltage, each current value is checked by increasing the gate bias voltage control bit one by one starting from 0. After the current value falls within the desired range, the gate bias voltage control bit is saved at that moment. Then, the next nanopore is selected, and the same operation is performed. At the end of calibration, gate bias voltage control bits are stored to allow a set current to flow for each nanopore, automatically recalling the stored control bits when each nanopore is selected so that the current flowing is the same.

F. ADC block diagram

Fig. 7. illustrates the changes in current when the Gate Bias voltage is altered, which is graphed in real time on the GUI. It reads 16-bit digitized data every second with chips and SPI communication and updates it to the display. In the graph, one data is plotted every second, and the y-axis can select digital data, voltage, and current, and the voltage and

current are obtained using Equation (1), (2) below.

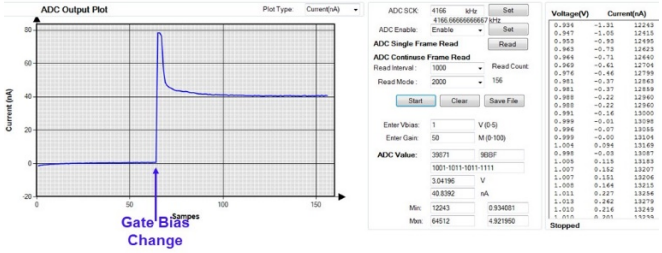

Fig. 7. Current change according to virus input.

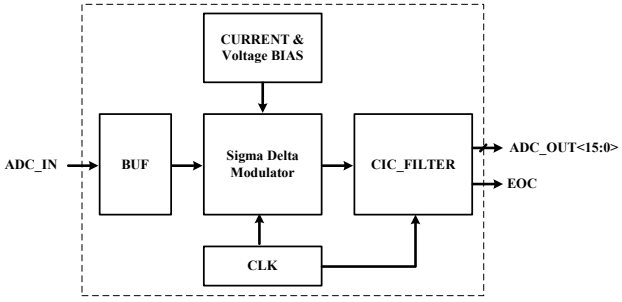

Fig. 8. Block diagram of Sigma-Delta ADC

The high-resolution ADC converts the bio sensor's signal to digital and delivers it to the external environment. The PGA output, adjusted for the ADC input range, is inputted into the Sigma-Delta modulation through a buffer. The serial output data of sigma delta modulation is output at a final 16-bit high resolution through the CIC Filter. Sampling clock for modulation and CIC filter is provided externally and properly divided and supplied. Through this, the bio sensor signal is used as a digital value in the final external environment. Fig. 8. is a block diagram of the Sigma-Delta ADC described above.

III. Results and Discussion

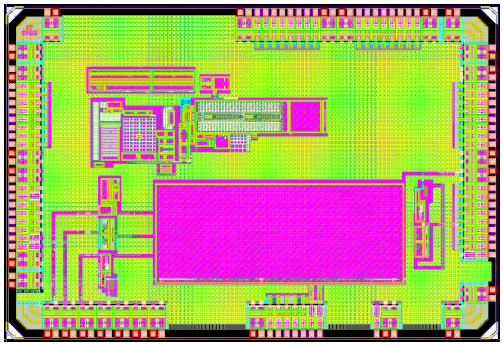

Fig. 9. Layout of the proposed current sensing system.

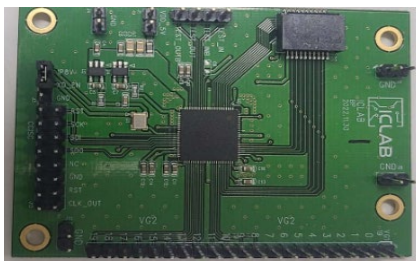

Fig. 10. Measurement board of the proposed current sensing system.

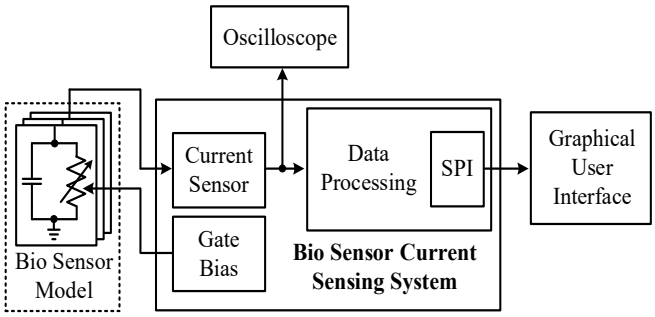

Fig. 11. Test lab environment of the proposed current sensing system.

The proposed current sensing system is fabricated in a 130 nm CMOS process. The chip micrograph is shown in Fig. 9, where it can be seen that the area is 3370 mm × 5000 mm. The experimental setup used to measure the current sensing system performance, which includes a bio sensor, is illustrated in Fig. 10., Fig. 11 shows the actual test lab environment. A biosensor model was constructed to measure the current sensing system. The biosensor model consists of a capacitor and a variable resistor whose resistance changes according to the applied voltage. The current input to the ASIC is converted into voltage, digitized, processed, and transmitted to the computer using SPI communication. The data delivered to the computer can be plotted by selecting among digital data, output voltage, and input current through the self-made GUI.

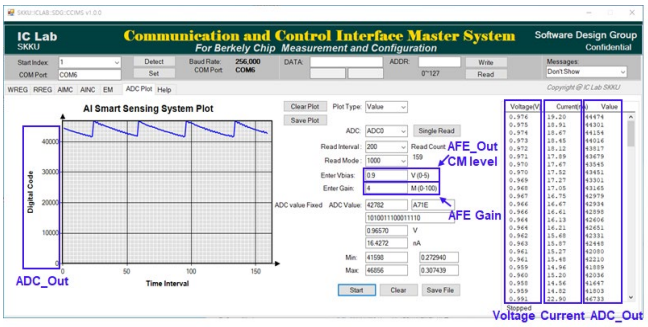

Fig. 12. GUI of the proposed current sensing system.

Fig. 12. illustrates a GUI that receives ASIC output data and indicates waveform, voltage, and current values. It receives 16-bit data from the ADC and converts it into a decimal number from 0 to 65,536, and displays it as a real-time graph. With this, the voltage and current can be checked in real time by changing the y-axis of the real-time graph into AFE output voltage or sensor's output current. It is possible to convert ADC 16-bit data into voltage and current using AFE gain and output common mode voltage level which are designed. The formula is as follows.

$$AFE\_Out = \frac{ADC\_data}{65535} + VDD/2 \quad (1)$$

$$Input\ Current = \frac{AFE_{Out} - AFE_{Out_{CM_{level}}}}{AFE_{Gain}} \quad (2)$$

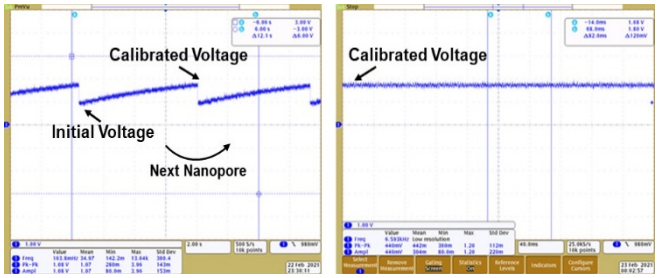

(a) (b)

Fig. 13. (a) Graph of the voltage storage process, (b) Graph of equalized base current.

Fig. 13. shows the measurement result of the gate bias voltage during nanopore calibration. By changing the gate bias voltage, when the current sensed at the nanopore approaches the set current value, the gate bias voltage at this time is stored. The same operation is performed on all nanopores to store the calibrated gate control bits in each nanopore. After calibration, the gate control bits stored in each of the actual measurement steps of each nanopore are loaded to equalize the base current of all nanopores.

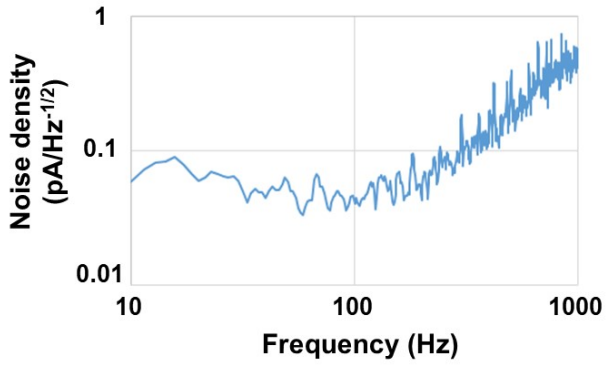

Fig. 14. Current change according to virus input.

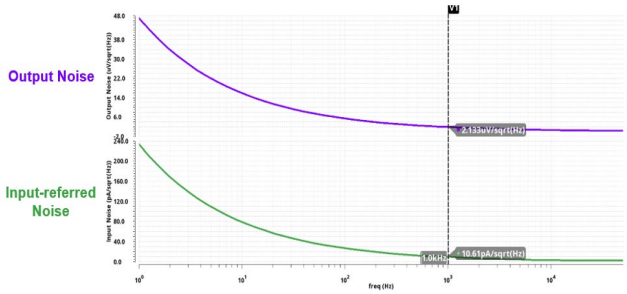

Fig. 15. AFE Noise Simulation.

Fig. 14. shows the input-referred noise performance of the TIA. The TIA's gain is 160 dBΩ and its bandwidth is 100 Hz. At frequency range from 10 Hz to 1000 Hz, when the root mean square value was obtained, which squared and added all noise density values and then took the square root, the input-referred noise of 4 pArms was confirmed. Fig. 15. shows the results of AFE's noise simulation.

TABLE I. Design implementation summary

Parameter	Value
AFE Gain	160 dBΩ
AFE bandwidth	1 kHz
Input-referred noise	4 pArms
ADC resolution	16 bit
Current consumption	10 mA
Process	130 nm CMOS
area	3.37 mm × 5 mm

TABLE I summarizes the implementation characteristics of the design. The proposed ASIC has a gain of 160 dBΩ and an input reference performance of 4 pArms at bandwidth of 1 kHz. ADC resolution is 16-bit, and the power consumption of the architecture is 10 mA from 1.5 V voltage source. This ASIC is designed with 130 nm CMOS process. The ASIC layout size is 3.37 mm × 5 mm.

IV. CONCLUSIONS

This paper proposes a biosensor current sensing system which amplifies the current output signal from a nanopore sensor, and converts it into digital data, enabling plotting and analyzing it in real time. The proposed biosensor current sensing system used resistive feedback for sensor voltage bias and actual resistance instead of pseudo resistance for low input reference noise. By applying the fixed values of gain and ADC input common mode voltage, the current signal data digitized after ADC can be displayed as the current value output from the sensor.

The biosensor current sensing system proposed in this paper has an input reference noise of 4 pArms at 160 dBΩ gain and 1 kHz bandwidth. It operates at an input voltage of 1.5 V, consuming a current of 10 mA.

ACKNOWLEDGMENT

The chip fabrication and EDA tool were supported by the IC Design Education Center (IDEC), South Korea.

REFERENCES

[1] K. Y. Goud; C. Moonla; R. K. Mishra; C. Yu; R. Narayan; I. Litvan; J. Wang, “Wearable electrochemical microneedle sensor for continuous monitoring of levodopa: toward parkinson management,” ACS Sens., vol.4, no.8, pp.2196-2204, Aug. 2019.

[2] Z. Zhang; M. Li; Y. Zuo; S. Chen; Y. Zhuo; M. Lu; G. Shi; H. Gu, “In vivo monitoring of pH in subacute PD mouse brains with a ratiometric electrochemical microsensor based on poly(melamine) films,” ACS Sens. vol.7, no.1, pp.235-244, Dec. 2021.

[3] N. S. Galenkamp; M. Soskine; J. Hermans; C. Wloka; G. Maglia, “Direct electrical quantification of glucose and asparagine from bodily fluids using nanopores,” Nat. Commun., vol.9, no., pp.4085, Oct. 2018.

[4] A. E. Chavis; K. T. Brady; G. A. Hatmaker; C. E. Angevine; N. Kothalawala; A. Dass; J. W. F. Robertson; J. E. Reiner, "Single molecule nanopore spectrometry for peptide detection," ACS Sens., vol.2, no.9, pp.1319-1328, Aug. 2017.

[5] J. -S. Yu; S. C. Hong; S. Wu; H. -M. Kim; C. Lee; J. -S. Lee; J. E. Lee; K. -B. Kim, "Differentiation of selectively labeled peptides using solid-state nanopores," Nanoscale, vol.11, no., pp.2510-2520, Jan. 2019.

[6] H. Niu; M. -Y. Li; Y. -L. Ying; Y. -T. Long, "An engineered third electrostatic constriction of aerolysin to manipulate heterogeneously charged peptide transport," Chem. Sci., vol.13, no., pp.2456-2461, Feb. 2022.

[7] Y. Wu; J. J. Gooding, "The application of single molecule nanopore sensing for quantitative analysis," Chem. Soc. Rev., vol.51, no., pp.3862-3885, May 2022.

[8] W. Si; H. Yang; G. Wu; Y. Zhang; J. Sha, "Velocity control of protein translocation through a nanopore by tuning the fraction of benzenoid residues," Nanoscale, vol.13, no., pp.15352-15361, Aug. 2021.

[9] S. -C. Liu; Y. -L. Ying; W. -H. Li; Y. -J. Wan; Y. -T. Long, "Snapshotting the transient conformations and tracing the multiple pathways of single peptide folding using a solid-state nanopore," Chem. Sci., vol.12, no., pp.3282-3289, Jan. 2021.

[10] D. F. Cairns-Gibson; S. L. Cockroft, "Funtionalised nanopores: chemical and biological modifications," Chem. Sci., vol.13, no., pp.1869-1882, Dec. 2021.

[11] S. Oh; M. -K. Lee; S. -W. Chi, "Single-molecule analysis of interaction between p53TAD and MDM2 using aerolysin nanopores," Chem. Sci., vol.12, no., pp.5883-5891, Mar. 2021.

[12] G. Seo; G. Lee; M. J. Kim; S. -H. Baek; M. Choi; K. B. Ku; C. -S. Lee; S. Jun; D. Park; H. G. Kim; S. –J. Kim; J. -O. Lee; B. T. Kim; E. C. Park; S. I. Kim, "Rapid detection of COVID-19 causative virus (SARS-CoV-2) in human nasopharyngeal swab specimens using field-effect transistor-based biosensor," ACS Nano., vol.14, no.4, pp.5135-5142, Apr. 2020.

[13] H. Yan; Z. Zhang; T. Weng; L. Zhu; P. Zhang; D. Wang; Q. Liu, "Recognition of bimolecular logic operation pattern based on a solid-state nanopore," Sensors, vol.21, no.1, pp.33, Dec. 2020.

[14] M. Hiratani; R. Kawano, "DNA logic operation with nanopore decoding to recognize microRNA patterns in small cell lung cancer," Anal. Chem., vol.90, no.14, pp.8531-8537, Jun. 2018.

[15] L. Xue; P. Cadinu; B. P. Nadappuram; M. Kang; Y. Ma; Y. Korchev; A. P. Ivanov; J. B. Edel, "Gated single-molecule transport in double-barreled nanopores," ACS Appl. Mater. Interfaces, vol.10, no.44, pp.38621-38629, Oct. 2018.

[16] E. B. Kalman; O. Sudre; I. Vlassiouk; Z. S. Siwy, "Control of ionic transport through gated single conical nanopores," Anal. Bioanal. Chem., vol.394, no., pp.413-419, May. 2009.

Sung Jae Lee received his B.S. degree from the Department of Electrical and Electronis Engineering at Konkuk University, Seoul, Korea, in 2023. He is currently working toward the Combined Ph.D & M.S. course in School of Electronics and Computer Engineering from Sungkyunkwan University, Suwon, Korea. His research interests include Power Management IC.

Sang Hyun Lee received his B.S. degree from the Department of Physics & Semiconductor Science at Dongguk University, Seoul, Korea, in 2023. He is currently working toward the M.S. course in Electronics and Computer Engineering from Sungkyunkwan University, Suwon, Korea. His research interests include RF.

Han Min Song received his B.S. degree from the Department of Chemical Engineering at Sungkyunkwan University, Suwon, Korea in 2021, He is currently working toward the combined Ph.D. & M.S. Course in Electornics and Computer Engineering from Sungkyunkwan University, Suwon, Korea. His research interests include ADC.

Sung June Byun received the B.S. de gree in electrical engineering from Inh a University, Incheon, in 2019. He is currently doing his combined Master's and Ph.D. degree at Sungkyunkwan U niversity, Suwon, South Korea. His res earch interests include CMOS Analog Circuit.

Kang-Yoon Lee received the B.S., M.S. and Ph.D. degrees in the School of Electrical Engineering from Seoul National University, Seoul, Korea, in 1996, 1998, and 2003, respectively.

From 2003 to 2005, he was with GCT Semiconductor Inc., San Jose, CA, where he was a Manager of the Analog Division and worked on the design of CMOS frequency synthesizer for CDMA/PCS/PDC and single-chip CMOS RF chip sets for W-CDMA, WLAN, and PHS. From 2005 to 2011, he was with the Department of Electronics Engineering, Konkuk University as an Associate Professor. Since 2012, he has been with College of Information and Communication Engineering, Sungkyunkwan University, where he is currently a Professor. His research interests include implementation of power integrated circuits, CMOS RF transceiver, analog integrated circuits, and analog/digital mixed-mode VLSI system design.